NJC

On–site formation of small Ag nanoparticles on superhydrophobic mesoporous silica for antibacterial application

COMMUNICATION

On-site formation of small Ag nanoparticles on superhydrophobic mesoporous silica for antibacterial application

Yang Zhu,[a] Chunhua Wu,[*b] Kazuyoshi Kanamori,[a] Toshiyuki Kamei,[c] Toyoshi Shimada[e] and Kazuki Nakanishi [*d,e]

A superhydrophobic mesoporous silica material loaded with on-site formed small Ag nanoparticles has been prepared via surface modification with octadecylsilane ($C_{18}H_{37}SiH_3$) and subsequent reduction of silver acetate with residual hydrido groups on-site. The resultant material shows excellent antibacterial activity for Gram-negative *E. coli* and Gram-positive *S. aureus*.

The appearance of new strains of bacteria resistant to current antibacterial agent has become a serious problem in public healthcare.[1-2] Simple, efficient, sustainable and cost-effective technologies to develop new and broad spectrum of bactericides are becoming increasingly demanded.[3] Among these technologies, developing antibacterial materials with superhydrophobicity has become a very hot topic in antibacterial design through bio-inspired and environmental friendly concepts.[4-5] It is well known that hydrophobicity of bactericide is beneficial to enhance the diffusion into cell membranes. Together with the synergistic effect from their unique layered shape, graphene and derivatives due to their high hydrophobicity can work as "nanoknives" to effectively penetrate cell membranes and therefore strongly inhibit the growth of microbial pathogens.[6] Based on such synergistic effect, many novel antibacterial agents were designed such as hydrophobic polymers, peptides with antibacterial terminis[7-9] and the hybrid systems of hydrophobic components with antibacterial agents such as Ag.[10-11] Further merits available from hydrophobicity are controlled release of antibacterial agents in aqueous media due to the water repellency as well as other extended functions such as anti-fouling and oil/water separation.[12-14]
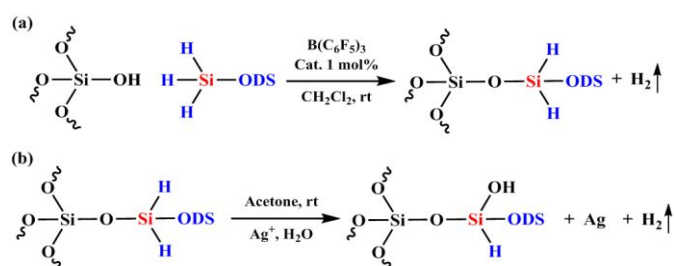
Scheme 1 (a) Surface functionalization of SBA-15 with octadecylsilane, (b) reduction of Ag^+ into Ag NPs by residual hydrido groups on ODS-H-SBA-15 surface.

Because of their high surface area, well-defined pore structure, high stability and modifiable surface, mesoporous silica has been used as a versatile platform to load various kinds of functional components for advanced applications.[15-17] Among them, Ag nanoparticles (NPs)[18-20] and hydrophobic organic groups[21] have been loaded separately into mesoporous silica-based materials for antibacterial applications. However, to the best of our knowledge, reports on the introduction of both antibacterial Ag NPs and hydrophobic organic groups to mesoporous silica are scarce. Furthermore, tedious and relatively inefficient multi-step reactions are commonly needed to achieve such multifunctional mesoporous materials by conventional surface modification methods.

a. Department of Chemistry, Graduate School of Science, Kyoto University, Kitashirakawa, Sakyo-ku, Kyoto, 606-8502, Japan.
b. College of Food Science, Fujian Agriculture and Forestry University, Fuzhou 350002, China.
c. Nara National College of Technology, 22-Yata-cho, Yamatokoriyama, Nara 639-1080, Japan.
d. Institute of Materials and Systems for Sustainability, Nagoya University, Furo-cho, Chikusa-ku, Nagoya, Aichi 464-8601, Japan.
e. Institute for Integrated Cell-Material Sciences, Kyoto University, Yoshida, Sakyo-ku, Kyoto 606-8501, Japan.
† Electronic Supplementary Information (ESI) available. See DOI: 10.1039/x0xx00000x
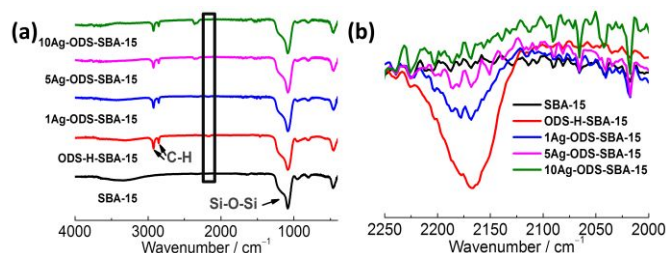
COMMUNICATION

Fig. 1 (a) FT-IR spectra and (b) magnified FT-IR spectra at the part labeled by the black square of SBA-15, ODS-H-SBA-15, 1Ag-ODS-SBA-15, 5Ag-ODS-SBA-15 and 10Ag-ODS-SBA-15.

Recently we have demonstrated a simple, versatile and highly efficient surface modification method for silica materials using a dehydrogenative reaction between surface silanols and mono-hydrosilanes ($R^1R^2R^3SiH$) activated by tris(pentafluorophenyl)borane $B(C_6F_5)_3$.[22] Herein, we for the first time show a one-step surface functionalization method to achieve a superhydrophobic/redox-active (octadecyl/hydrido) bifunctional mesoporous material (denoted as ODS-H-SBA-15 hereafter) by extending the reaction to a tri-hydrosilane, (octadecylsilane, $C_{18}H_{37}SiH_3$, Scheme 1a) using SBA-15 as the host (Brunauer-Emmett-Teller (BET) surface area: 560 m^2 g^{-1}, specific pore volume: 0.60 cm^3 g^{-1}, modal pore diameter: 6.3 nm, Fig. S1a,b and Table S1, ESI†). The resulting bifunctional surface is then used to reduce Ag^+ on-site and form silica-supported small Ag NPs with controlled particle size, homogeneous spatial distribution and close proximity to superhydrophobic octadecyl groups. The obtained mesoporous material (denoted as XAg-ODS-SBA-15 hereafter, where X represents the starting concentration of the Ag source, silver acetate) bearing both superhydrophobicity and antibacterial activity can work efficiently towards antibacterial applications.

As shown in Fig. 1a, b, FT-IR spectra confirm the successful functionalization of the silica surface with octadecylsilane. The two resolved peaks corresponding to C-H vibration at *ca.* 2922 and 2854 cm^{-1} are observed, suggesting the presence of octadecyl groups in ODS-H-SBA-15, in comparison with the spectrum of bare SBA-15. Such observation is consistent with the result of TG analysis in Figure S2, where around 25 % of weight loss in the temperature range of 250-600 °C, corresponding to the pyrolysis of octadecyl groups in ODS-H-SBA-15. The presence of residual Si-H groups on the surface of SBA-15 is revealed from the Si-H stretching peak at ca. 2166 cm^{-1} (Fig. 1b). Since the concentration of silanol groups on the surface of SBA-15 calcined at 600 °C is sufficiently low, further reactions between the residual hydrido groups and a neighboring silanol is unlikely to occur after the reaction between one of the hydrido groups of the silane and a silanol. As a result, the residual hydrido groups remain intact after the surface functionalization. The loading of octadecyl groups in the SBA-15 is 0.88 mmol g^{-1} (C content: 19.1 wt%) as determined by CHN elemental analysis. This amount is smaller than that obtained on HPLC standard spherical silica beads (BET surface area: 414 m^2 g^{-1}, specific pore volume: 1.1 cm^3
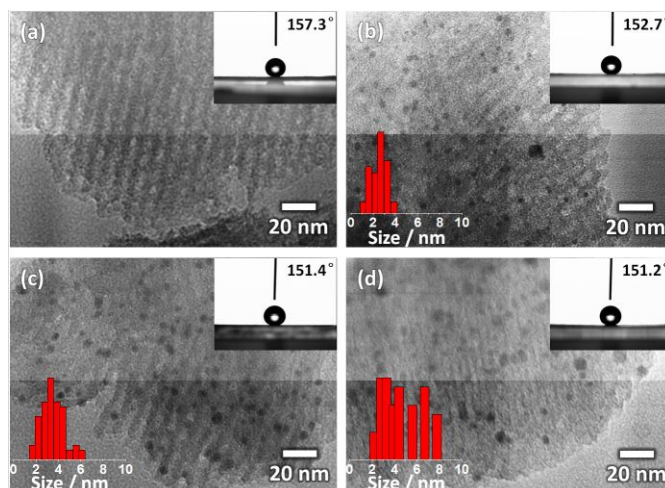

Fig. 2 TEM images of (a) ODS-H-SBA-15, (b) 1Ag-ODS-SBA-15, (c) 5Ag-ODS-SBA-15 and (d) 10Ag-ODS-SBA-15 (inset of the images shows contact angles on the superhydrophobic surfaces and Ag NPs size distribution obtained from the TEM images).

g^{-1}, median pore diameter: 10.0 nm, octadecyl loading: 1.06 mmol g^{-1}, C content: 25.4 wt%) modified by octadecyldimethylsilane on MCM-41 (BET surface area: 850 m^2 g^{-1}) in our previous report,[21] but higher than that of standard commercial product (C content: 11.7 wt%, ODS-4, GL Sciences, Inc., Saitama, Japan), which again proves the higher efficiency of the present surface modification method than the conventional ones typically utilizing chloro- or alkoxysilanes, for the functionalization of silica materials. The reason for lower loading compared to our previous work,[21] despite an expected higher reactivity of octadecylsilane than dimethyloctadecylsilane, lies in the lower BET surface area of SBA-15 (560 m^2 g^{-1}, vs. 850 m^2 g^{-1} for MCM-41). Much smaller TG weight loss indicating lower octadecyl loading is observed when dimethyloctadecylsilane is used for the modification of SBA-15 surface following the same procedure (Fig. S2, ESI†). Figures S1c,d and Table S1 show a drastic decrease of micro/mesoporosity and total pore volume, and a concomitant decrease in BET surface area (from 560 m^2 g^{-1} to 40 m^2 g^{-1}) and modal pore size (from 6.3 nm to 4.3 nm). These results suggest that octadecylsilane molecules are attached on the surface of micropores and mesopores, especially given the fact that the mesostructure of the material remains intact as confirmed by transmission electron microscopy (TEM, Fig. 2a). The bulkiness of octadecyl groups restricts the access to a part of the micropores and reduces the size of the mesopores. Nevertheless, due to the presence of large amount of octadecyl groups, the silica surface becomes superhydrophobic with the water contact angle as 157 °. The superhydrophobicity remains stable at least for 20 s with no evident change of measured water contact angle.

Such superhydrophobicity results in much less water adsorption on both the outer and inner surface of the ODS-H-SBA-15 than bare SBA-15 as is indicated from the negligible weight loss in the temperature range < 100 °C in Fig. S2, ESI†.

COMMUNICATION

Table 1 MIC values (µg mL^{-1}) of SBA-15-based materials against *E. coli* and *S. aureus*.

| Bacteria	SBA-15	ODS-H-SBA-15	5Ag-ODS-SBA-15
E.coli	>1000	>1000	62.50
S.aureus	>1000	500	3.91

The residual hydrido groups in ODS-H-SBA-15 are then used to reduce Ag$^+$ into NPs onsite on the mesopore wall. Silver acetate (AgOAc) was used as the Ag$^+$ source due to its moderate solubility in water/acetone mixed solvent, through which the redox reaction kinetics between hydrido groups and Ag$^+$ can be controlled. After dissolution, solvated AgOAc can diffuse into the mesopores of SBA-15, and dissociation is followed by the redox reaction on the pore surfaces. Dissociation of AgOAc releases Ag$^+$, which will be reduced by the embedded hydrido groups immediately. A homogeneous distribution of small Ag NPs both inside and outside the mesoporous particles can therefore be expected. When the concentration of AgOAc is low (0.1 mmol L^{-1}), the reaction is completed in less than 1 min judging from the color change of the SBA-15 particles, forming small Ag NPs (average diameter ca. 3 nm) inside the mesopores

with a narrow particle size distribution (Fig. 2b insets). However, due to the low concentration of AgOAc, the loading of Ag in 1Ag-ODS-SBA-15 was low judging from almost negligible UV-Vis absorption around 450 nm and X-ray diffraction (Fig. S3, ESI†) and confirmed from the result of Inductively Coupled Plasma-Mass Spectroscopy (ICP-MS) as 1.4 wt%. As the concentration of AgOAc is increased to 0.5 mmol L^{-1} and further to 1 mmol L^{-1}, increased amounts of Ag NPs embedded inside the mesopores are observed and the average particle size remains as 3 nm due to the spatial confinement by the cylindrical mesopores. In the meantime, some NPs located outside the mesopores grow in size, resulting in a broader size distribution of Ag NPs (Figures 2c, d). As more Ag$^+$ is reduced by the residual hydrido groups, the loading of Ag increases along with the increase of the concentration of AgOAc as indicated by the diminishing FT-IR vibration peak of the hydrido groups in Figure 1b and increased intensities of UV-Vis absorption and X-ray diffraction corresponding to Ag NPs in Figure S3, and also the loading of Ag revealed from ICP-AES as 6 wt% and 6.7 wt% for 5Ag-ODS-SBA-15 and 10Ag-ODS-SBA-15, respectively.

As is demonstrated in Scheme 1b, the reduction of Ag$^+$ produces silanols simultaneously at the hydrido site, which therefore increases the hydrophilicity of the silica surface. A slight decrease of superhydrophobicity indicated by the decrease of water contact angle is thus observed as more Ag$^+$ is reduced (Fig. 2 insets). Note that the surface of SBA-15 remains superhydrophobic (water contact angle > 150 °) even after the completion of the redox reaction and the formation of significant amount of silanols. Since the octadecyl groups remain unaffected after the redox reaction between hydrido
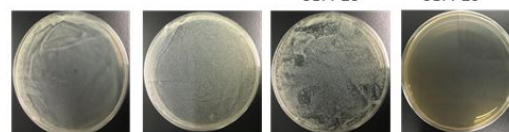
Fig. 3 Antibacterial activities of SBA-15-based materials.

groups and Ag$^+$, their bulkiness can still shield the as-formed silanols as well as those located nearby, from the contact of water.

The chemical state of Ag in 10Ag-ODS-SBA-15 was probed by X-ray photoelectron spectroscopy (XPS, Fig. S4, ESI†). Deconvoluted doublet peaks at binding energies of 374.2 eV and 368.2 eV with a spin energy separation of 6.0 eV due to Ag 3d$_{3/2}$ and Ag 3d$_{5/2}$ of metallic Ag are observed.[23-24] Peaks corresponding to ionic Ag are found negligible in the XPS spectrum, indicating the absence of unreacted AgOAc in the sample.

To ascertain the antibacterial activity of the SBA-15-based samples, 5Ag-ODS-SBA-15 with an optimal Ag loading and a relatively homogeneous particle size distribution was chosen and two typical pathogen bacteria, including a Gram-negative bacteria *Escherichia coli O157:H7* (*E. coli*, ATCC2 5922) and a Gram-positive Bacteria *Staphylococcus aureus* (*S. aureus*, KCTC 1928) were used as the test strain in the present study. We first investigated how bacteria respond to our system in solution and determined the minimum inhibitory concentration (MIC). As demonstrated in Table 1, the growth inhibition effect of Ag-loaded superhydrophobic SBA-15 against *S. aureus* and *E. coli* is observed, while normal SBA-15 does not show any antibacterial activity. It can be observed that no visible *S. aureus* growth on Lurie Broth (LB) medium containing as low as 3.91 µg mL^{-1} of 5Ag-ODS-SBA-15, while 62.50 µg mL^{-1} of 5Ag-ODS-SBA-15 is required to fully inhibit the growth of *E. coli*, indicating that the *S. aureus* is more susceptible to Ag-loaded superhydrophobic SBA-15 than *E. coli*. This difference might be derived from different cell surface conditions of the bacterial membrane.[26] It should be noted that the ODS-H-SBA-15 showed slight antibacterial activity for *S. aureus* but no evident antibacterial activity for *E. coli*. However, the superhydrophobic character can offer some favorable properties such as controlled release of Ag$^+$ as strong antibacterial agent via a reduced contact of Ag NPs with dissolved molecular oxygen,[2, 3, 25] inhibited bacterial adhesion and easy separation of the antibacterial agents from aqueous media, which may lead to a persistent surface antibacterial capability for the present bifunctional materials. Besides, in contrast to the previously reported Ag-SiO$_2$ nanocomposites (which is typically 10-1000 µg mL^{-1} for *E. coli* and 100-2000 µg mL^{-1} for *S. aureus*),[2,20,27,28] the present bifunctional materials

exhibit an excellent antibacterial activity for *E. coli* and *S. aureus*.

To further confirm the antibacterial properties of the SBA-15-based materials, the colony-forming count method was also applied for quantitative evaluation. As shown in Figure 3, the presence of 5Ag-ODS-SBA-15 in the LB-agar plates could completely inhibit the formation of colonies for both types of bacteria, while SBA-15 and ODS-H-SBA-15 did not demonstrate antibacterial activity for *E. coli* and *S. aureus*, which is consistent with the results from the MIC analyzed.

In conclusion, a trihydrosilane octadecylsilane has been applied to the surface modification of mesoporous silica for the first time to achieve a superhydrophobic/redox-active (octadecyl/hydrido) bifunctional material. The residual hydrido groups are then used for the on-site formation of small Ag NPs homogeneously distributed in the mesopores. The resultant superhydrophobic mesoporous silica loaded with small Ag NPs shows excellent antibacterial activity towards Gram-negative bacteria *E. coli* and Gram-positive bacteria *S. aureus*. Such synthetic method can be further extended by other hydrosilanes toward the fabrication of multifunctional systems for various applications.

Conflicts of interest

There are no conflicts to declare.

Acknowledgements

Notes and references

1   B. Chudasama, A. K. Vala, N. Andhariya, R. V. Upadhyay and R. V. Mehta, *Nano Res.*, 2010, **2**, 955-965.
2   S. Chernousova and M. Epple, *Angew. Chem. Int. Ed.*, 2013, **52**, 1636-1653.
3   L.   Rizzello and P. P. Pompa, *Chem. Soc. Rev.*, 2014, **43**, 1501-1518.
4   T. Liu, B. Yin, T. He, N. Guo, L. Dong and Y. Yin, *ACS Appl. Mater. Interfaces*, 2012, **4**, 4683-4690.
5   M. Zhang, P. Wang, H. Sun and Z. Wang, *ACS Appl. Mater. Interfaces*, 2014, **6**, 22108-22115.
6   X. Zou, L. Zhang, Z. Wang and Y. Luo, *J. Am. Chem. Soc.*, 2016, **138**, 2064-2077.
7   M. Zasloff, *Nature*, 2002, **415**, 389-395.
8   Y.   Chen, M. T. Guarnieri, A. I. Vasil, M. L. Vasil, C. T. Mant and R. S. Hodges, *Antimicrob. Agents Chemther.*, 2007, **51**, 1398-1406.
9   P. Li, Y. F. Poon, W. Li, H. Y. Zhu, S. H. Yeap, Y. Cao, X. Qi, C. Zhou, M. Lamrani, R. W. Beuerman, E. T. Kang, Y. Mu, C. M. Li, M. W. Chang, S. S. Leong and M. B. Chan-Park, *Nat. Mater.*, 2011, **10**, 149-156.
10 M. Wu, B. Ma, T. Pan, S. Chen and J. Sun, *Adv. Funct. Mater.*, 2016, **26**, 569-576.
11 R.   Liu, Y. Y. Lee, K. S. L. Chong and N. Tomczak, *Adv. Mater. Interfaces*, 2016, **3**, 1500448.
12 D. Rana and T. Matsuura, *Chem. Rev.*, 2010, **110**, 2448-2471.
13 Z.   Xue, Y. Cao, N. Liu, L. Feng, L. Jiang, *J. Mater. Chem. A*, 2014, **2**, 2445-2460.
14 L. Zhang, L. Zhang, Y. Yang, W. Zhang, H. Lv, F. Yang, C. Lin, P. Tang, *J. Biomed. Mater. Res. B*, 2016, **104B**, 1004-1012.
15 I. I. Slowing, B. G. Trewyn, S. Giri and V. S. Y. Lin, *Adv. Funct. Mater.*, 2007, **17**, 1225-1236.
16 R.   Ciriminna, A. Fidalgo, V. Pandarus, F. Beland, L. M. Ilharco and M. Pagliaro, *Chem. Rev.*, 2013, **113**, 6592-6620.
17 F.   Hoffmann, M. Cornelius, J. Morell and M. Froba, *Angew. Chem. Int. Ed.*, 2006, **45**, 3216-3251.
18 V.   Ambrogi, A. Donnadio, D. Pietrella, L. Latterini, F. A. Proietti, F. Marmottini, G. Padeletti, S. Kaciulis, S. Giovagnoli and M. Ricci, *J. Mater. Chem. B*, 2014, **2**, 6054-6063.
19 L. Wang, H. He, C. Zhang, L. Sun, S. Liu and R. Yue, *J. Appl. Microbiol.*, 2014, **116**, 1106-1118.
20 Y.   Tian, J. Qi, W. Zhang, Q. Cai and X. Jiang, *ACS Appl. Mater. Interfaces*, 2014, **6**, 12038-12045.
21 E. Pedziwiatr-Werbicka, K. Milowska, M. Podlas, M. Marcinkowska, M. Ferenc, Y. Brahmi, N. Katir, J. P. Majoral, A. Felczak, A. Boruszewska, K. Lisowska, M. Bryszewska and A. El Kadib, *Chem. Eur. J.*, 2014, **20**, 9596-9606.
22 N.   Moitra, S. Ichii, T. Kamei, K. Kanamori, Y. Zhu, K. Takeda, K. Nakanishi and T. Shimada, *J. Am. Chem. Soc.*, 2014, **136**, 11570-11573.
23 P. Weightman and P. T. Andrews, *J. Phys. C: Solid State Phys.*, 1980, **13**, 3529.
24 Y.   Liu, R. G. Jordan and S. L. Qiu, *Phys. Rev. B*, 1994, **49**, 4478-4484.
25 B. Reidy, A. Hasse, A. Luch, K. A. Dawson, I. Lynch, Materials, 2013, 6, 2295-2350.
26 J.   Tang, Q. Chen, L. Xu, S. Zhang, L. Feng, L. Cheng, H. Xu, Z. Liu and R. Peng, *ACS Appl. Mater. Interfaces*, 2013, **5**, 3867-3874.
27 Y.   Hu, K. Cai, Z. Luo, K. D. Jandt, *Adv. Mater.* 2010, **22**, 4146-4150.
28 Y. H. Kim, D. K. Lee, H. G. Cha, C. W. Kim and Y. S. Kang, *J. Phys. Chem. C*, 2007, **111**, 3629-3635.